Single-molecule nanocatalysis reveals heterogeneous reaction pathways and catalytic dynamics

WEILIN XU, JASON S. KONG, YUN-TING E. YEH AND PENG CHEN*

Department of Chemistry and Chemical Biology, Cornell University, Ithaca, New York 14853, USA
***e-mail: pc252@cornell.edu**

Published online: 9 November 2008; doi:10.1038/nmat2319

Nanoparticles are important catalysts for many chemical transformations. However, owing to their structural dispersions, heterogeneous distribution of surface sites and surface restructuring dynamics, nanoparticles are intrinsically heterogeneous and challenging to characterize in ensemble measurements. Using a single-nanoparticle single-turnover approach, we study the redox catalysis of individual colloidal Au nanoparticles in solution, using single-molecule detection of fluorogenic reactions. We find that for product generation, all Au nanoparticles follow a Langmuir–Hinshelwood mechanism but with heterogeneous reactivity; and for product dissociation, three nanoparticle subpopulations are present that show heterogeneous reactivity between multiple dissociation pathways with distinct kinetics. Correlation analyses of single-turnover waiting times further reveal activity fluctuations of individual Au nanoparticles, attributable to both catalysis-induced and spontaneous dynamic surface restructuring that occurs at different timescales at the surface catalytic and product docking sites. The results exemplify the power of the single-molecule approach in revealing the interplay of catalysis, heterogeneous reactivity and surface structural dynamics in nanocatalysis.

Nanoparticles made of various materials can catalyse many chemical transformations in organic synthesis, pollutant removal and energy production; intense efforts are made to characterize the structures and catalytic properties of nanoparticle catalysts[1–16]. Although structures of individual nanoparticles can be studied down to atomic resolution with advanced transmission electron microscopy (TEM) and scanning-probe microscopies[4,8,10–14], their catalytic properties have been measured mainly at the ensemble level[4–9,11,12,16], obtaining averaged properties. The catalytic properties of nanoparticles are intrinsically heterogeneous, however, owing to their structural dispersions, heterogeneous distribution of surface sites and surface restructuring dynamics[4,13–15,17,18]. This intrinsic heterogeneity can cause both nanoparticle-dependent and temporally varying catalytic properties. Therefore, to address this heterogeneity challenge, it is highly desired to interrogate nanoparticle catalysis at the single-nanoparticle level in real time, preferably with single-turnover resolution. Using surface plasmon spectroscopy, Novo *et al.* recently observed the steady-state accumulation of redox reactions catalysed by single Au nanocrystals[19]. Here, we study the real-time redox catalysis of single colloidal Au nanoparticles at the single-turnover level with millisecond time resolution, using single-molecule detection of fluorogenic reactions[20–24].

We discovered that spherical colloidal Au nanoparticles can catalyse the fluorogenic reduction of non-fluorescent resazurin to highly fluorescent resorufin by NH_2OH (see Supplementary Information, Figs S1,S2). This fluorogenic reaction provides the basis for studying real-time single-Au-nanoparticle catalysis by detecting the fluorescence of the catalytic product resorufin at the single-molecule level. To monitor individual Au nanoparticles (6.0 ± 1.7 nm) catalysing this reaction, we immobilized them on an amine-functionalized, positively charged glass surface and flowed the substrate solution over (0.05–1.2 μM resazurin and 1 mM NH_2OH) (Fig. 1a). Using a total internal reflection fluorescence microscope with up to 30 ms frame rate and 532 nm laser excitation, we recorded movies of stochastic fluorescence bursts at many localized spots on the glass surface (Fig. 1b and Supplementary Information, Movie S1). A typical time trajectory of fluorescence intensity from one of these spots contains stochastic off–on signals that span the entire movie (~67 min, Fig. 1c, Supplementary Information, Fig. S4). The digital nature of the trajectory and the consistent height of the on-level indicate each fluorescence burst comes from a single resorufin molecule—were it from many molecules, the bursts would have variable heights depending on the number of molecules.

We attributed the single-resorufin fluorescence bursts to single catalytic turnovers by a single Au nanoparticle. On a single-molecule basis, the event of a chemical reaction occurs on the subpicosecond timescale and cannot be resolved here. Consequently, each product formation event on the nanoparticle surface appears as a sudden intensity increase in the fluorescence trajectory, each product dissociation event appears as a sudden intensity decrease and each off–on cycle corresponds to a single turnover of a catalytic formation of a product and its subsequent dissociation on one particle. The dissociated product molecules in solution are undetectable at our imaging speed owing to their fast diffusion.

Many observations support our conclusion (see Supplementary Information, Figs S5,S6). (1) No digital fluorescence bursts are observed in the absence of Au nanoparticles, or resazurin or NH_2OH. (2) Flowing resorufin solution (up to ~10^{-8} M) over

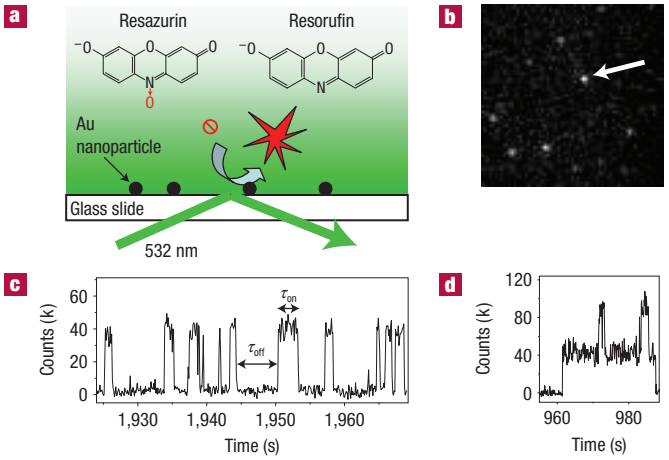

Figure 1 Single-turnover detection of single-Au-nanoparticle catalysis. **a**, Experimental design using total internal reflection fluorescence microscopy. **b**, A typical image ($\sim 18 \times 18\,\mu m^2$) of fluorescent products during catalysis taken at 100 ms per frame. The pixel size is ~270 nm, which results in the pixelated fluorescence spots. **c**, A segment of the fluorescence trajectory from the fluorescence spot marked by the arrow in **b** at 0.05 μM resazurin and 1 mM NH_2OH. **d**, A segment of another fluorescence trajectory showing two on-levels at the same conditions.

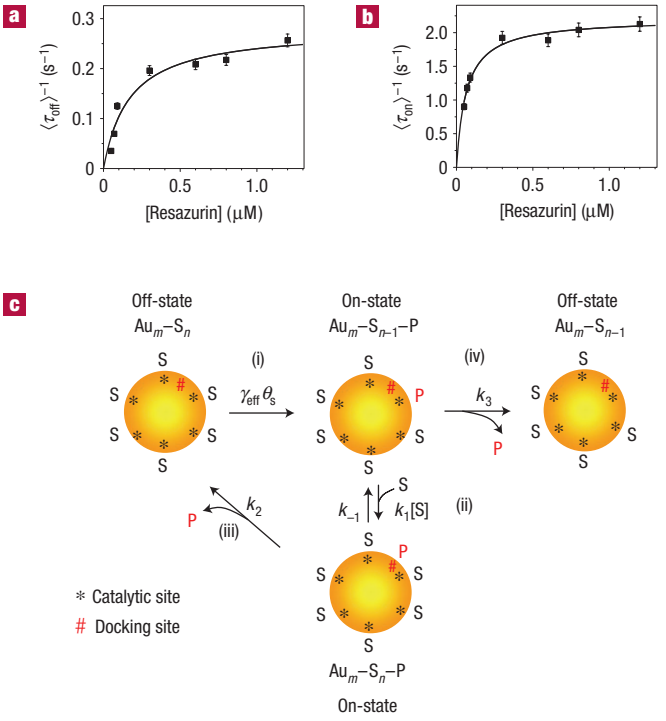

Figure 2 Kinetic mechanism of catalysis. **a**,**b**, Resazurin concentration dependence of $\langle\tau_{off}\rangle^{-1}$ (**a**) and $\langle\tau_{on}\rangle^{-1}$ (**b**). Each data point is an average from >50 trajectories, each of which contains hundreds of turnovers. Solid lines are fits with equations (1) and (2) with $\gamma_{eff} = 0.28 \pm 0.02\,s^{-1}$, $K_1 = 6 \pm 2\,\mu M^{-1}$, $k_2 = 2.2 \pm 0.1\,s^{-1}$, $K_2 = 16 \pm 2\,\mu M^{-1}$ and $k_3 = 0 \pm 3\,s^{-1}$. Note here the values of the kinetic parameters are the average of many nanoparticles. Errors are s.d. Note here the values of K_1, k_2, K_2 and k_3 represent the reactivity per site averaged over all of the sites on one nanoparticle. All error bars in the graphs are s.e.m. All experiments are in 1 mM NH_2OH. **c**, Schematic diagram of the kinetic mechanism. Au_m: Au nanoparticle; S: resazurin; P: resorufin. Au_m–S_n represents a Au nanoparticle having *n* adsorbed substrate molecules. The fluorescence state (on or off) of the nanoparticle is indicated at each reaction stage.

Au nanoparticles does not yield fluorescence bursts, indicating neither diffusion of free resorufin, nor resorufin binding/unbinding to a Au nanoparticle, nor fluorescence blinking of nanoparticle-bound resorufin is responsible for the bursts. (3) The burst frequencies are independent of laser intensity; the fluorescence bursts are thus not photoinduced. (4) The average τ_{on} is much shorter than the photobleaching lifetime (~25 s) of resorufin at the laser intensity used; therefore, the intensity decrease in the fluorescence trajectories is not due to resorufin photobleaching. (5) The number density of fluorescence spots in our movies is $\sim 0.035\,\mu m^2$. Assuming a Poisson distribution, the probability of having multiple Au nanoparticles is <0.06% within $1 \times 1\,\mu m^2$, which is an easily obtainable resolution of our microscope. We thus attributed the catalytic turnovers in one trajectory to a single Au nanoparticle: each turnover comes from one of the many possible active sites on the surface of the nanoparticle.

In some turnover trajectories, ~1% of the fluorescence bursts show multiple on-levels (Fig. 1d). This indicates a new resorufin molecule is generated on the nanoparticle surface before an earlier one dissociates away. The percentage (~20%) of this type of trajectories is greater than the probability (<0.06%) of having multiple nanoparticles within a localized fluorescence spot ($\sim 1 \times 1\,\mu m^2$, Fig. 1b). Thus, these multilevel events directly reflect the multitude of either catalytic sites that can undertake catalysis parallely, or docking sites where products can stay on the Au nanoparticle surface before dissociation.

Although the actual events of catalytic product formation or product dissociation are instantaneous and appear as intensity jumps in the fluorescence trajectories with our millisecond time resolution, the time needed (the 'waiting time') for substrate diffusion, binding or thermal activation before such an event is usually much longer. The τ_{off} and τ_{on} are the two waiting times in these single-turnover fluorescence trajectories (Fig. 1c). Resolving them enables us to probe the kinetic mechanism of catalysis in two parts separately: τ_{off} is the waiting time before each resorufin formation; τ_{on} is the waiting time for resorufin dissociation after its formation; their individual values are stochastic, but their statistical properties, such as average values and distributions, are well defined by the underlying reaction kinetics. Statistically, $\langle\tau_{off}\rangle^{-1}$ and $\langle\tau_{on}\rangle^{-1}$, where $\langle\,\rangle$ denotes averaging, represent the time-averaged single-particle rates of product formation and of product dissociation, respectively. When averaged over the turnover trajectories from many Au nanoparticles, $\langle\tau_{off}\rangle^{-1}$, the catalytic product formation rate, is expectedly dependent on the resazurin concentration [S] and exhibits saturation kinetics (Fig. 2a). Surprisingly, $\langle\tau_{on}\rangle^{-1}$, the product dissociation rate, also shows [S]-dependent kinetics; this indicates that the substrate participates in product dissociation (Fig. 2b).

To focus on the resazurin reduction and to understand quantitatively the catalytic kinetics, we approximated that the explicit term for NH_2OH can be omitted from the kinetic mechanism, as NH_2OH does not affect the kinetics at large excess (1 mM, Supplementary Information, Fig. S7). The [S] dependence of the product formation rate $\langle\tau_{off}\rangle^{-1}$ can then be described by a Langmuir–Hinshelwood mechanism for heterogeneous catalysis[25], in which the nanoparticle catalyses the substrate conversion to product while maintaining a fast substrate adsorption equilibrium (Fig. 2c, reaction (i)). If *k* is the rate constant for one catalytic site and *n* is the number of substrates adsorbed on

the surface catalytic sites of a nanoparticle, then the reaction rate for forming one product on one nanoparticle is kn (see Supplementary Information). The Langmuir adsorption isotherm dictates $n = n_T\theta_S = n_T K_1[S]/(1 + K_1[S])$, where n_T is the total number of surface catalytic sites on one Au nanoparticle, θ_S is the fraction of occupied catalytic sites and K_1 is the substrate adsorption equilibrium constant. Following a single-molecule kinetic analysis (see Supplementary Information), we get the single-molecule Langmuir–Hinshelwood equation:

$$\langle\tau_{off}\rangle^{-1} = \frac{1}{\int_0^\infty \tau f_{off}(\tau)\mathrm{d}\tau} = kn_T\theta_S = \frac{\gamma_{eff}K_1[S]}{1+K_1[S]}, \qquad (1)$$

where $f_{off}(\tau)$ is the probability density function of τ_{off}, and $\gamma_{eff} = kn_T$ and represents the combined reactivity of all surface catalytic sites on one Au nanoparticle. Equation (1) connects τ_{off}, a stochastic single-molecule quantity, with conventional kinetic parameters and predicts the saturation kinetics of $\langle\tau_{off}\rangle^{-1}$. Fitting the nanoparticle-averaged data in Fig. 2a gives $\gamma_{eff} = 0.28 \pm 0.02\,s^{-1}$ and $K_1 = 6 \pm 2\,\mu M^{-1}$, both values here reflecting averaged properties of many Au nanoparticles.

To account for the [S] dependence of the product dissociation rate $\langle\tau_{on}\rangle^{-1}$, we considered a substrate-assisted product dissociation pathway, involving a pre-substrate-binding step (Fig. 2c, reactions (ii), (iii)), besides direct dissociation (Fig. 2c, reaction (iv)). The equation connecting $\langle\tau_{on}\rangle^{-1}$ with conventional kinetic parameters is (see Supplementary Information):

$$\langle\tau_{on}\rangle^{-1} = \frac{1}{\int_0^\infty \tau f_{on}(\tau)\mathrm{d}\tau} = \frac{k_2K_2[S]+k_3}{1+K_2[S]}, \qquad (2)$$

where $f_{on}(\tau)$ is the probability density function of τ_{on}, k_2 is the rate constant of product dissociation in the substrate-assisted pathway (reaction (iii)), k_3 is the rate constant of direct product dissociation (reaction (iv)) and $K_2 = k_1/(k_{-1} + k_2)$ (Fig. 2c). When $[S] \to 0$, $\langle\tau_{on}\rangle^{-1} \to k_3$, because no substrate is available to drive the product dissociation to the substrate-assisted pathway and direct product dissociation dominates. When at saturating [S], $\langle\tau_{on}\rangle^{-1}$ approaches k_2, because high [S] drives the product dissociation towards the substrate-assisted pathway. Fitting the nanoparticle-averaged data in Fig. 2b gives $k_2 = 2.2 \pm 0.1\,s^{-1}$, $K_2 = 16 \pm 2\,\mu M^{-1}$ and $k_3 = 0 \pm 3\,s^{-1}$. Clearly, k_3, the direct dissociation pathway, is un-identifiable here in nanoparticle-averaged results.

On a single-nanoparticle basis, equation (1) predicts the catalytic product formation rate $\langle\tau_{off}\rangle^{-1}$ to show variable saturation levels and initial slopes with increasing [S], if different Au nanoparticles have heterogeneous catalytic reactivity (γ_{eff}) and substrate binding affinity (K_1) (Fig. 3a). From equation (2), the product dissociation rate $\langle\tau_{on}\rangle^{-1}$ can have three types of kinetic behaviour if Au nanoparticles have heterogeneous reactivity between the two product dissociation pathways (Fig. 3b): (I) asymptotic increase with increasing [S] if the nanoparticle has $k_2 > k_3$, that is, the nanoparticle prefers the substrate-assisted dissociation pathway; (II) asymptotic decrease if $k_2 < k_3$, that is, the nanoparticle prefers the direct dissociation pathway; and (III) constant at any [S] if $k_2 = k_3$ or $K_2 = 0$. To probe if heterogeneous reactivity exists among Au nanoparticles, we measured the catalysis for the same set of Au nanoparticles over three resazurin concentrations (microscope drifting and catalyst deactivation over extended time limit the number of concentrations in our experiment (see Supplementary Information, Fig. S13)). The catalytic product formation rates $\langle\tau_{off}\rangle^{-1}$ from individual nanoparticles reveal distinct saturation levels and initial slopes with increasing [S] (Fig. 3a). More excitingly, the product dissociation rates $\langle\tau_{on}\rangle^{-1}$ from individual nanoparticles show

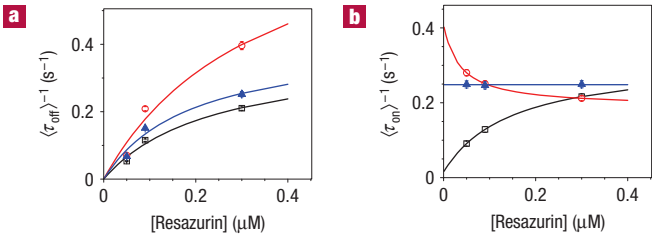

Figure 3 Heterogeneous reactivity in catalysis and reaction pathways. **a**,**b**, Resazurin concentration dependence of $\langle\tau_{off}\rangle^{-1}$ (**a**) and $\langle\tau_{on}\rangle^{-1}$ (**b**) from three single Au nanoparticles of type-I (square), type-II (circle) and type-III (filled triangle). Solid lines are simulations of equations (1) and (2): for the type-I nanoparticle, $\gamma_{eff} = 0.38\,s^{-1}$, $K_1 = 4.3\,\mu M^{-1}$, $k_2 = 3.2\,s^{-1}$, $K_2 = 6.7\,\mu M^{-1}$ and $k_3 = 0.15\,s^{-1}$; for the type-II nanoparticle, $\gamma_{eff} = 0.86\,s^{-1}$, $K_1 = 2.9\,\mu M^{-1}$, $k_2 = 1.8\,s^{-1}$, $K_2 = 28\,\mu M^{-1}$ and $k_3 = 4.1\,s^{-1}$; for the type-III nanoparticle, $\gamma_{eff} = 0.41\,s^{-1}$, $K_1 = 5.3\,\mu M^{-1}$, $k_2 = k_3 = 2.4\,s^{-1}$ (or $k_2 = 0$) and $K_2 =$ arbitrary value. All error bars in the graphs are s.e.m. All experiments are in 1 mM NH_2OH.

all three types of [S] dependence with different subpopulations (Fig. 3b): 66% of Au nanoparticles are type-I, 19% are type-II and 15% are type-III. These diverse behaviours reflect the nanoparticles' heterogeneous reactivity in catalysis and their differential reactivity between parallel reaction pathways, both of which are hidden in nanoparticle-averaged results (Fig. 2a,b and Supplementary Information, Fig. S8). In particular, for $\langle\tau_{on}\rangle^{-1}$, type-I nanoparticles dominate the averaged behaviours. However, by examining single-nanoparticle kinetics, our measurements here unmask their heterogeneous reactivity both in catalysis and in reaction pathways.

From each single-turnover trajectory, we further determined the time dependence of the rate of turnovers (the number of off–on cycles per unit time) (Fig. 4a). Large temporal variations were observed, indicating dynamic activity fluctuations of individual Au nanoparticles. The activity fluctuations could be due to reaction rate changes in the τ_{off} reaction (the catalytic product formation), the τ_{on} reaction (the product dissociation), or both. To separate the contributions of τ_{off} and τ_{on} reactions to the activity fluctuations, we extracted the sequence of individual τ_{off} and that of individual τ_{on} from each turnover trajectory, and then calculated their autocorrelation functions $C_\tau(m) = \langle\Delta\tau(0)\Delta\tau(m)\rangle/\langle\Delta\tau^2\rangle$ (refs 26,27). Here, τ is either τ_{off} or τ_{on}, m is the turnover index number in the sequence and $\Delta\tau(m) = \tau(m) - \langle\tau\rangle$, where $\langle\ \rangle$ denotes averaging. In the presence of activity fluctuations, $C_\tau(m) \geqslant 0$ and shows a decay behaviour with the decay time constant being the fluctuation correlation time[26,27].

For one Au nanoparticle at a saturating [S] (1.2 μM), both $C_{\tau_{off}}(m)$ and $C_{\tau_{on}}(m)$ show an exponential decay, indicating both τ_{off} and τ_{on} reaction rates fluctuate (Fig. 4b,c). The decay constants are $m_{off} = 12.5 \pm 2.9$ and $m_{on} = 2.6 \pm 0.9$ turnovers. With an average turnover time of ~4.5 s for this turnover trajectory, the fluctuation correlation times for the τ_{off} and τ_{on} reactions are ~56 and ~12 s, respectively. These two correlation times reflect the fluctuation timescales of γ_{eff} and k_2, which are rate-limiting in τ_{off} and τ_{on} reactions at saturating resazurin concentrations (Fig. 2c). The insets in Fig. 4b,c show the histograms of the fluctuation correlation time of τ_{off} and τ_{on} reactions from many Au nanoparticles; their broad distributions indicate that the activity fluctuations of different Au nanoparticles can have very different timescales.

These dynamic fluctuations of activity are not photoinduced because their correlation times are independent of laser excitation (see Supplementary Information, Fig. S9). Moreover, TEM did

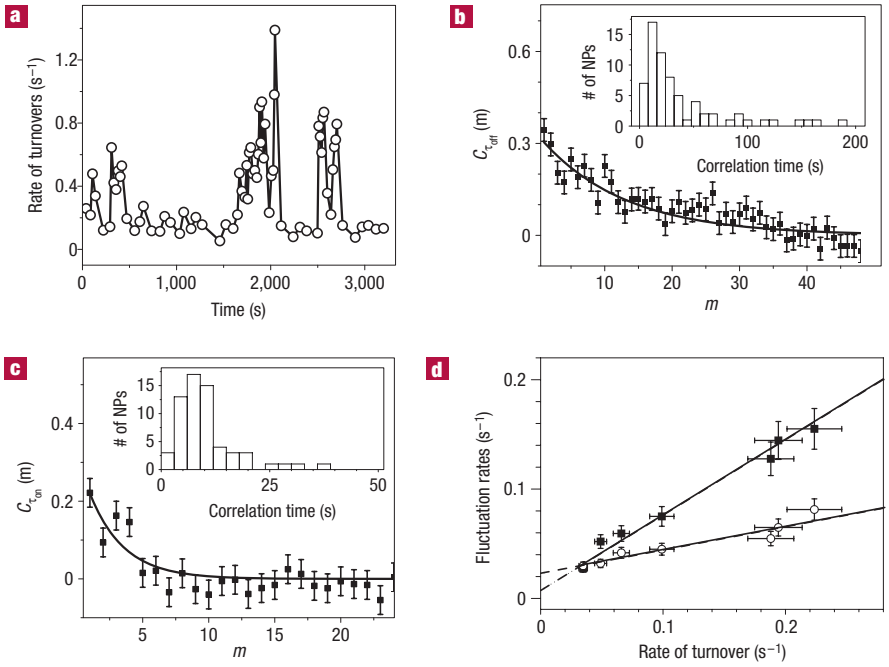

Figure 4 Single-nanoparticle catalytic dynamics. a, Trajectory of rate of turnovers for a single Au nanoparticle at 1.2 μM resazurin. Data points are calculated every 10 turnovers. **b**,**c**, Autocorrelation functions of τ_{off} (**b**) and τ_{on} (**c**) derived from the same single-turnover trajectory as that in **a**. Solid lines are exponential fits with decay constants of $m_{off} = 12.5 \pm 2.9$ and $m_{on} = 2.6 \pm 0.9$ turnovers. Insets: Histograms of fluctuation correlation times for τ_{off} and τ_{on} reactions at 1.2 μM resazurin. NPs: nanoparticles. **d**, Dependence of the activity fluctuation rate (the inverse of fluctuation correlation time) on the rate of turnovers. Circles represent the τ_{off} reaction and squares represent the τ_{on} reaction. Each data point is an average from >50 trajectories. Error bars are s.d. Solid lines are linear fits.

not reveal discernible morphology changes of Au nanoparticles after catalysis (see Supplementary Information, Fig. S3). We attributed the activity fluctuations to small-scale dynamic surface restructuring that occurs throughout the many surface sites of a Au nanoparticle. Dynamic surface restructuring is well known for metal nanoparticles and bulk metals in heterogeneous catalysis[13–15,17,18,28]; the changing adsorbate–surface interactions during catalysis can induce dynamic surface reconstruction, causing oscillatory kinetics due to different activities of different surface structures[18,28,29]. For the Au nanoparticles here, dynamic surface restructuring can change $\gamma_{eff} (= kn_T)$ by altering the reactivity per catalytic site k or the total number of surface catalytic sites n_T for τ_{off} reactions; it can change k_1, k_2 or k_3, the rate constants per site for τ_{on} reactions; both will lead to temporal fluctuations of activity. Consequently, the fluctuation correlation times of activity are the timescales of the surface restructuring dynamics at the relevant surface sites. The inverses of the correlation times, that is, the fluctuation rates, are then the corresponding surface restructuring rates, which should increase with faster rates of catalytic turnovers.

To support our attribution, we determined the dependence of the activity fluctuation rates on the rate of turnovers. For all Au nanoparticles, the fluctuation rates increase with increasing rates of turnovers (Fig. 4d and Supplementary Information, Fig. S10), directly supporting the catalysis-induced nature of the activity fluctuations and the surface restructuring as the underlying cause. This dependence also ruled out substrate migration among different surface sites as the cause, because substrate migration should diminish at high rates of turnovers where all sites are occupied owing to high [S] (see Supplementary Information).

In addition, we note the clear difference between the two fluctuation rates at the highest rate of turnovers (Fig. 4d), where, owing to high [S], γ_{eff} and k_2 dominate τ_{off} and τ_{on} reactions. This difference in fluctuation rates indicates that γ_{eff} and k_2 experience distinct surface restructuring dynamics. Moreover, no cross-correlation between τ_{off} and τ_{on} was detectable at high [S] (see Supplementary Information, Fig. S11). We thus conclude that on each nanoparticle, the catalytic sites, where the catalytic reaction γ_{eff} occurs, are different from the docking sites, where the dissociation reaction k_2 occurs (Fig. 2c).

The distinction between the catalytic and docking sites on the nanoparticle surface provides hints on the nature of the activity differences among type-I, II and III nanoparticles, which differ in their relative magnitudes of k_2 and k_3 (Fig. 3b). The direct product dissociation reaction k_3 occurs from the catalytic sites (reaction (iv), Fig. 2c), as compared with the docking sites for k_2. Therefore, the different activities of the three types of nanoparticle reflect the different properties (possibly slightly different structures) of their surface catalytic sites and product docking sites.

We further extrapolated the fluctuation rates linearly to zero rate of turnovers (Fig. 4d and Supplementary Information, Fig. S10). The positive intercepts (0.023 ± 0.003 and $0.007 \pm 0.004\ s^{-1}$ in Fig. 4d) approximate the rates of spontaneous (as compared with catalysis-induced) surface restructuring dynamics for a Au nanoparticle in solution, corresponding to a timescale of about 40–150 s. Although we cannot factor out the solvent contributions, the determination of a timescale for nanoparticle surface restructuring dynamics in the absence of catalysis is exciting, as they are in general challenging to quantify owing to the nanometre dimension and the heterogeneous surface structure of nanoparticles.

By examining single-nanoparticle catalysis in real time at single-turnover resolution, this study exemplifies the power of the

single-molecule approach in revealing the interplay of catalysis, heterogeneous reactivity and surface structural dynamics in nanocatalysts. We expect our approach here is applicable to study many other nanoparticle catalysts, including differentiating the reactivity of different-sized Au nanoparticles (see Supplementary Information, Fig. S17), and more insights into nanocatalysis are to emerge from similar single-molecule studies.

METHODS

Spherical colloidal Au nanoparticles prepared from citrate reduction of $HAuCl_4$ in aqueous solutions were either purchased (Ted Pella) or made in-house[30], and characterized by TEM (FEI Tecnai 12) at Cornell Centre for Materials Research. Single-molecule fluorescence experiments were carried out on a homebuilt prism-type total internal reflection microscope (Olympus IX71)[31]. A continuous-wave circularly polarized 532 nm laser (CrystaLaser) of 1.5–3 mW was focused onto an area of $\sim 80 \times 40\,\mu m^2$ on the sample to directly excite the fluorescence of the product resorufin. The fluorescence of resorufin was collected by a $\times 60$ NA 1.2 water-immersion objective (Olympus), filtered by two filters (Chroma Technology) and projected onto an EMCCD camera (Andor Technology), which is controlled by Andor IQ software. An extra $\times 1.6$ magnification on the microscope is also used sometimes. The movies are analysed using a home-written IDL program, which extracts the individual fluorescence intensity trajectories from localized fluorescence spots across the entire movie. The intensity of each bright spot in an image is obtained by integrating the signal counts over an area of $\sim 1 \times 1\,\mu m^2$.

A flow cell, $100\,\mu m \times 2\,cm \times 5\,mm$, formed by double-sided tape sandwiched between a quartz slide (Technical Glass or Finkenbeiner) and a borosilicate coverslip (Gold Seal), was used to hold aqueous sample solutions for single-nanoparticle single-molecule fluorescence measurements. Before being assembled into a flow cell, the quartz slide was amine-functionalized by an aminoalkylsiloxane reagent (Vectabond, Vector Laboratory), the amine functional group of which is protonated, thus positively charged in water. 100 µl of 1 nM colloidal Au nanoparticle solution was then added onto the slide, and incubated for 30 min. The slide was then rinsed with nanopure water to wash away the unbound Au nanoparticles. These colloidal Au nanoparticles were prepared from citrate reduction of $HAuCl_4$; they are negatively charged and known to be immobilized on positively charged surfaces[30,32,33]. On the quartz slide, two holes were drilled to connect to polyethylene tubing and a syringe pump for continuous solution flow at $5\,\mu l\,min^{-1}$.

Received 11 March 2008; accepted 14 October 2008; published 9 November 2008.

References

1. Somorjai, G. A., Contreras, A. M., Montano, M. & Rioux, R. M. Clusters, surfaces, and catalysis. *Proc. Natl Acad. Sci. USA* **103**, 10577–10583 (2006).
2. Ertl, G., Knözinger, H. & Weitkamp, J. *Handbook of Heterogeneous Catalysis* (VCH, 1997).
3. Bell, A. T. The impact of nanoscience on heterogeneous catalysis. *Science* **299**, 1688–1691 (2003).
4. Burda, C., Chen, X., Narayanan, R. & El-Sayed, M. A. Chemistry and properties of nanocrystals of different shapes. *Chem. Rev.* **105**, 1025–1102 (2005).
5. Heiz, U. & Landman, U. (eds) *Nanocatalysis* (Springer, 2007).
6. Bond, G. C., Louis, C. & Thompson, D. T. (eds) *Catalysis by Gold* (Imperial College Press, 2006).
7. Crooks, R. M., Zhao, M., Sun, L., Chechik, V. & Yeung, L. K. Dendrimer-encapsulated metal nanoparticles: Synthesis, characterization, and application to catalysis. *Acc. Chem. Res.* **34**, 181–190 (2001).
8. Chen, M. & Goodman, D. W. Catalytic active gold: From nanoparticles to ultrathin films. *Acc. Chem. Res.* **39**, 739–746 (2006).
9. Hughes, M. D. *et al.* Tunable gold catalysts for selective hydrocarbon oxidation under mild conditions. *Nature* **437**, 1132–1135 (2005).
10. Sun, Y. & Xia, Y. Shape-controlled synthesis of gold and silver nanoparticles. *Science* **298**, 2176–2179 (2002).
11. Lee, H. *et al.* Morphological control of catalytically active platinum nanocrystals. *Angew. Chem. Int. Ed.* **45**, 7824–7828 (2006).
12. Jaramillo, T. F. *et al.* Identification of active edge sites for electrochemical H_2 evolution from MoS_2 nanocrystals. *Science* **317**, 100–102 (2007).
13. Wang, Z. L. New developments in transmission electron microscopy for nanotechnology. *Adv. Mater.* **15**, 1497–1514 (2003).
14. Hansen, P. L. *et al.* Atom-resolved imaging of dynamic shape changes in supported copper nanocrystals. *Science* **295**, 2053–2055 (2002).
15. Newton, M. A., Belver-Coldeira, C., Martinez-Arias, A. & Fernandez-Garcia, M. Dynamic in situ observation of rapid size and shape change of supported Pd nanoparticles during CO/NO cycling. *Nature Mater.* **6**, 528–532 (2007).
16. Haruta, M., Yamada, N., Kobayashi, T. & Iijima, S. Gold catalysts prepared by coprecipitation for low-temperature oxidation of hydrogen and of carbon monoxide. *J. Catal.* **115**, 301–309 (1989).
17. Somorjai, G. A. *Introduction to Surface Chemistry and Catalysis* (Wiley–Interscience, 1994).
18. King, D. A. & Woodruff, D. P. (eds) *Phase Transitions and Adsorbate Restructuring at Metal Surfaces* (Elsevier, 1994).
19. Novo, C., Funston, A. M. & Mulvaney, P. Direct observation of chemical reactions on single gold nanocrystals using surface plasmon spectroscopy. *Nature Nanotechnol.* **3**, 598–602 (2008).
20. Edman, L., FiSldes-Papp, Z., Wennmalm, S & Rigler, R. The fluctuating enzyme: A single molecule approach. *Chem. Phys.* **247**, 11–22 (1999).
21. Velonia, K. *et al.* Single-enzyme kinetics of CAlB-catalyzed hydrolysis. *Angew. Chem. Int. Ed.* **44**, 560–564 (2005).
22. English, B. P. *et al.* Ever-fluctuating single enzyme molecule: Michaelis-Menton equation revisited. *Nature Chem. Biol.* **3**, 87–94 (2006).
23. Roeffaers, M. B. *et al.* Spatially resolved observation of crystal-face-dependent catalysis by single turnover counting. *Nature* **439**, 572–575 (2006).
24. Smiley, R. D. & Hammes, G. G. Single molecule studies of enzyme mechanisms. *Chem. Rev.* **106**, 3080–3094 (2006).
25. Satterfield, C. N. *Heterogeneous Catalysis in Practice* (McGraw-Hill, 1980).
26. Lu, H. P., Xun, L. Y. & Xie, X. S. Single-molecule enzymatic dynamics. *Science* **282**, 1877–1882 (1998).
27. Witkoskie, J. B. & Cao, J. Single molecule kinetics. I. Theoretical analysis of indicators. *J. Chem. Phys.* **121**, 6361–6372 (2004).
28. Imbihl, R. & Ertl, G. Oscillatory kinetics in heterogeneous catalysis. *Chem. Rev.* **95**, 697–733 (1995).
29. King, D. A. Nonlinear effects in adsorption and reaction dynamics at surfaces: Kinetic oscillations under scrutiny. *Surf. Rev. Lett.* **1**, 435–442 (1994).
30. Handley, D. A. in *Colloidal Gold: Principles, Methods, and Applications* (ed. Hayat, M. A.) 13–32 (Academic, 1989).
31. Sarkar, S. K. *et al.* Engineered Holliday junctions as single-molecule reporters for protein-DNA interactions with application to a MerR-family regulator. *J. Am. Chem. Soc.* **129**, 12461–12467 (2007).
32. Natan, M. J. & Lyon, L. A. Jr. in *Metal Nanoparticles: Synthesis, Characterization, and Application* (eds Feldheim, D. L. & Foss, C. A.) 183–205 (Dekker, 2002).
33. Grabar, K. C., Freeman, R. G., Hommer, M. B. & Natan, M. J. Preparation and characterization of Au colloid monolayers. *Anal. Chem.* **67**, 735–743 (1995).

Supplementary Information accompanies the paper at www.nature.com/naturematerials.

Acknowledgements

We thank Cornell University, ACS Petroleum Research Foundation (47918-G5) and Cornell Centre for Materials Research for financial support and J. Grazul for assistance in TEM.

Author contributions

P.C. designed experiments; W.X., J.S.K., Y.-T.E.Y. and P.C. carried out experiments; W.X., J.S.K. and P.C. analysed data; W.X. and P.C. wrote the paper.

Author information

Reprints and permissions information is available online at http://npg.nature.com/reprintsandpermissions. Correspondence and requests for materials should be addressed to P.C.